

# Reconstruction of electron beam distribution using phase-retrieval algorithm

Yong Woon Parc,<sup>a</sup> Changbum Kim,<sup>b\*</sup> Jung Yun Huang<sup>b</sup> and In Soo Ko<sup>a</sup>

<sup>a</sup>Department of Physics, Pohang University of Science and Technology, Pohang 790-784, Republic of Korea, and <sup>b</sup>Pohang Accelerator Laboratory, Pohang University of Science and Technology, Pohang 790-784, Republic of Korea. E-mail: chbkim@postech.ac.kr

Received 12 May 2010

Accepted 1 February 2011

The shapes of light sources such as electron beams can be reconstructed by inverse Fourier transformation of the complex degree of spatial coherency, which can be measured using Young's interferometer. The application of the phase-retrieval algorithm to reduce phase measurement errors in the complex degree of spatial coherency is numerically studied using an electron beam with an asymmetric distribution. This application is demonstrated with experimental data measured at the diagnostic beamline at the Pohang Accelerator Laboratory.

© 2011 International Union of Crystallography  
Printed in Singapore – all rights reserved

**Keywords:** coherency; interference; electron beam.

## 1. Introduction

Over the past several decades interferometer techniques have been successfully implemented to measure the size of an electron beam at various storage rings (Mitsuhashi, 1999; Sakai *et al.*, 2000; Fisher *et al.*, 2001; Masaki & Takano, 2003). Recently, numerical and experimental studies have improved the measurement techniques (Naito & Mitsuhashi, 2006; Parc *et al.*, 2009). The shape of an electron beam can be reconstructed by using the inverse Fourier transformation (IFT) of the complex degree of coherency, which can be measured by experiment. To determine the complex degree of coherency we need to measure the visibility and the phase of the interferogram (Mitsuhashi, 1999). In general, the IFT result for the shape of the electron beam is distorted owing to the measurement error of the phase. Mitsuhashi (1999) used the cosine Fourier transformation method to eliminate the phase measurement error. However, the application of this method is limited to symmetric distribution as in the case of the Gaussian shape of the electron beam (Mitsuhashi, 1999).

Alternatively, the size of an electron beam with a Gaussian distribution can be determined by comparing the measured spatial coherency and the numerically calculated coherency (Sakai *et al.*, 2000; Parc *et al.*, 2009). However, this method requires several trials to match the numerically calculated result with the measured result under the assumption of a Gaussian distribution for the electron beam. If the electron beam shape is not Gaussian, it is impossible to estimate the source shape by using this method. Therefore, it is highly desirable to find a method that eliminates the phase error in reconstructing the non-symmetric distribution of the electron beam.

In this paper we show that the phase-retrieval algorithm introduced by Fienup (1980) is appropriate for reconstructing

the distribution of an electron beam that is asymmetric. The phase information required to reconstruct an image from the measured diffractogram can be retrieved by using the algorithm. To demonstrate the application of this method in the electron beam diagnostics, the complex degree of spatial coherency of light generated from the Pohang Light Source (PLS) is investigated using the diagnostics beamline at the Pohang Accelerator Laboratory. The theory of interference and spatial coherency is reviewed in §2. A numerical study on the phase-retrieval algorithm and reconstructed image of the electron beam is described in §3. The experimental application of the phase-retrieval algorithm is presented in §4. Finally, a summary is provided in §5.

## 2. Theory

Using Young's interferometer the degree of correlation between two points in a wavefront generated from a light source can be investigated, as shown in Fig. 1. The degree of correlation is called the spatial coherency of light. The interferogram constructed by an interferometer with two slits is calculated as (Goodman, 1985)

$$I(P) = \left\langle \left| K_1 \tilde{u}\left(S_1, t - \frac{r_1}{c}\right) + K_2 \tilde{u}\left(S_2, t - \frac{r_2}{c}\right) \right|^2 \right\rangle, \quad (1)$$

where  $P$  is a point on the screen in Fig. 1,  $K_i$  is the amplitude of the wave at the slit  $S_i$  for  $i = 1$  and 2, and  $r_i$  is the distance from the slit  $S_i$  to the point  $P$ . If  $K_1$  and  $K_2$  are given by the same value  $K$ , equation (1) can be written as

$$I(P) = 2K^2 I_0 \left[ 1 + \left| \tilde{\gamma}\left(\frac{r_2 - r_1}{c}\right) \right| \cos\left(2\pi \bar{\nu} \frac{r_2 - r_1}{c} + \alpha\right) \right], \quad (2)$$

where  $I_0$  is the initial intensity of light as given by  $|\tilde{u}(t)|^2$ ,  $\tilde{\gamma}$  is the complex degree of spatial coherency,  $\bar{\nu}$  is the central

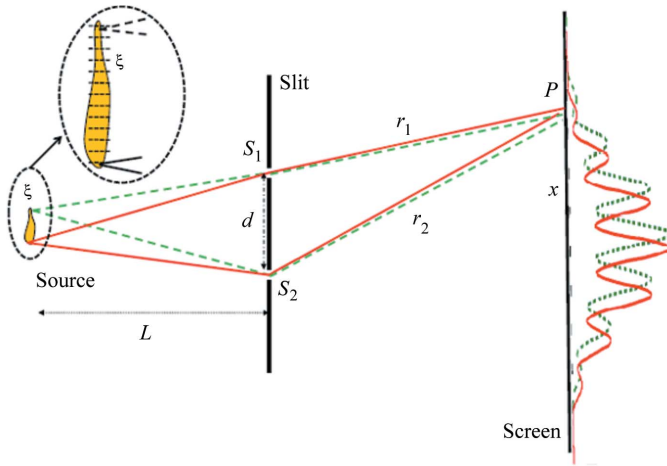


**Figure 1**  
Configuration of interference with finite-size light source.  $d$  is the distance between two slits.  $S_i$  is the slit position and  $r_i$  is the distance between points  $S_i$  and  $P$  on the screen for  $i = 1, 2$ .  $L$  is the distance between the source and the slit mask.

frequency of light,  $c$  is the speed of light in the air and  $\alpha$  is the phase of the interferogram. The visibility of the interferogram is defined as (Born & Wolf, 1999)

$$V = \frac{I_{\max} - I_{\min}}{I_{\max} + I_{\min}} = \left| \tilde{\gamma} \left( \frac{r_2 - r_1}{c} \right) \right|. \quad (3)$$

The spatial coherency of light from a finite-size source can be estimated from the van Cittert–Zernike theorem (Cittert, 1934; Zernike, 1938). When  $d$  is the distance between the slits, the van Cittert–Zernike theorem can be expressed as

$$\tilde{\gamma}(d) = \int_{\sigma} I(\xi) \exp\left(-ik \frac{d}{L} \xi\right) d\xi, \quad (4)$$

where the wavenumber  $k = 2\pi/\lambda$ ,  $\xi$  is the position of the infinitesimal light source, and  $L$  is the distance between the source and the slit. From (4), the complex degree of spatial coherency is revealed as the Fourier transform (FT) of the intensity distribution  $I$  of the light source (Sakai *et al.*, 2000; Parc *et al.*, 2009).

### 3. Numerical study

In our numerical model all infinitesimal fragments of the light source emit light independently (Parc *et al.*, 2009). For the numerical study of the interferogram the intensity of the interferogram on the screen can be calculated by taking into consideration all of the phase changes owing to the path differences from an infinitesimal fragment of the light source to a point  $P$  on the screen.

A numerically calculated interferogram with light (wavelength 650 nm) generated from a Gaussian distribution source is shown in Fig. 2. The points in Fig. 2 represent the numerical calculation results of the interferogram with a Gaussian light source. The inset of Fig. 2 shows the source distribution with a Gaussian shape, which is used in this numerical study. This Gaussian distribution will be used several times in this paper.

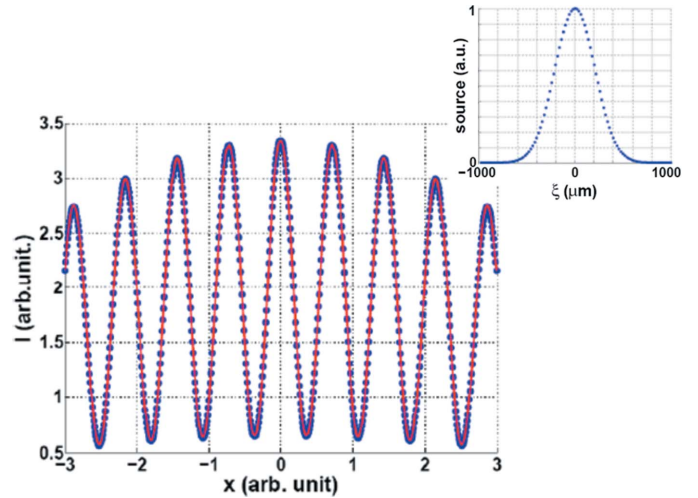


**Figure 2**  
The numerically calculated result of the interferogram is shown by dots. The solid line is the plot of the theory in equation (5). The distance between the slits  $d$  is 1 cm and the half slit width  $a$  is 300  $\mu\text{m}$ . The electron beam distribution used in this numerical study is shown in the inset. The standard deviation of the Gaussian distribution  $\sigma$  is 210  $\mu\text{m}$ .

The formula for the interferogram from the Gaussian shape source with two slits is given by the relation

$$I(P) = 2 \left[ \frac{\sin(u)}{u} \right]^2 \left[ 1 + \exp\left(-\frac{\sigma^2}{2} v^2\right) \cos(\delta + \alpha) \right], \quad (5)$$

with  $u = kax/R$ ,  $v = kd/L$  and  $\delta = kdx/R$ , where the wave-number  $k = 2\pi/\lambda$ ,  $a$  is the half-width of the slit,  $R$  is the distance between the center ( $O$ ) of the slits and a point ( $P$ ) on the screen,  $x$  is the distance of the observation point from the screen center,  $\sigma$  is the standard deviation of the Gaussian source,  $L$  is the distance between the source and the slit mask, and  $d$  is the distance between the two slits.

The solid line in Fig. 2 is the plot of equation (5) with the same parameters used in the simulation. The line in Fig. 2 is well matched with the interferogram from the numerical model. Thus, the theoretical and numerical models are in good agreement. In this numerical study the distance  $L$  between the source and the slit is 24.5 m, the slit distance  $d$  is set to 1.0 cm, the half-slit width  $a$  is 300  $\mu\text{m}$ , and the distance  $D$  between the slit and the screen is 12 km (Parc *et al.*, 2009).

#### 3.1. Amplitude and phase of FT

In this section the sum of two Gaussians is used to represent an asymmetric distribution of an electron beam, as shown in Fig. 3. The standard deviations of the two Gaussian distributions are 210  $\mu\text{m}$  ( $\sigma_1$ ) and 105  $\mu\text{m}$  ( $\sigma_2$ ) in Fig. 3. The separation of the two Gaussians ( $l$ ) is 420  $\mu\text{m}$ . Visibilities obtained from the numerical study are represented by circles in Fig. 4(a). The visibility is no longer Gaussian as shown in Fig. 4(a).

From equations (3) and (4) we can see that the amplitude of the FT of the electron beam distribution should be the same with this visibility. The amplitude of the FT of the same electron beam distribution used in the numerical study is plotted using dots in Fig. 4(a) to compare the numerically

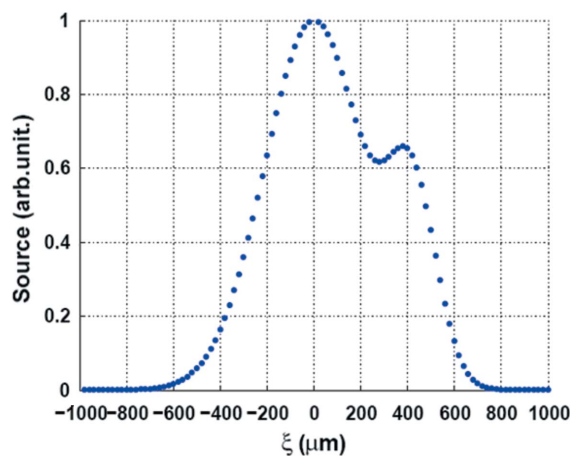


**Figure 3**  
 Electron beam distribution used in this numerical study. The standard deviation of one Gaussian distribution is 210  $\mu\text{m}$  and that of the other is 105  $\mu\text{m}$ . The distance between the centers of the two Gaussian distributions is 420  $\mu\text{m}$ .

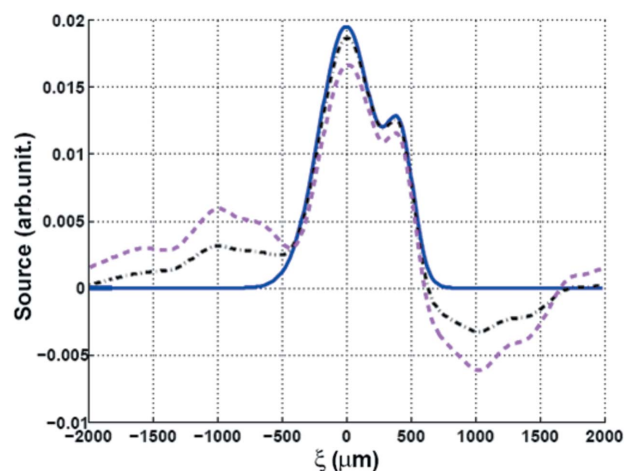
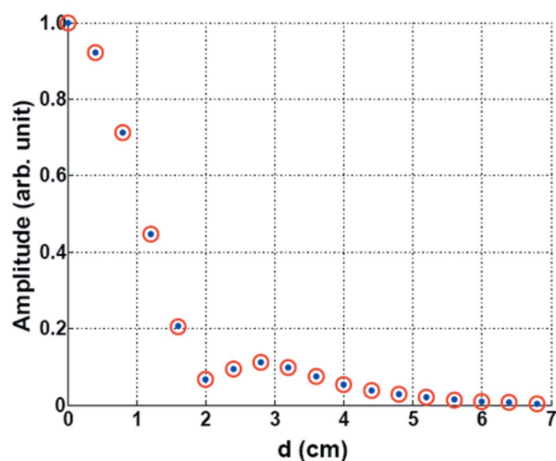
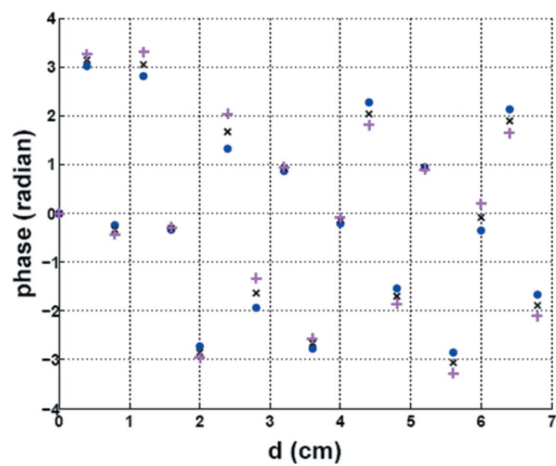


**Figure 5**  
 Electron beam shape obtained by IFT for the two Gaussians in Fig. 3. The solid line represents the result of IFT with the original phase. The dash-dotted (dashed) line represents the IFT result with random phase of a maximum value of 0.4 (0.8) rad.



(a)



(b)

**Figure 4**  
 (a) Visibility and amplitude of the FT of the distribution shown in Fig. 3. The circles are the numerically calculated visibilities. The dots are the amplitudes of the FT. (b) Phase of the FT. The dots are the original phases obtained from the FT results with the distribution in Fig. 3. The symbol  $\times$  (+) is used for random phases with a maximum value of 0.4 (0.8) rad.

calculated visibility. The numerically calculated visibility (circles) and the amplitude of the FT (dots) are closely matched.

The phases used in this section come from the FT of the electron beam distribution in the previous section. In the real experiment these will be measured from the interferograms. There will be some errors in the measurement result. These errors will provide distorted measurement results for a certain distribution of electron beams in a storage ring (Mitsuhashi, 1999). In Fig. 4(b) the original phases coming from the FT of Fig. 3 are shown by dots. To study the effects of the errors in the reconstruction of the electron beam, we assumed random errors in the original phase as shown in Fig. 4(b). Random errors within 0.4 (0.8) rad are added to the original phase, represented by the symbol  $\times$  (+).

### 3.2. The effect on IFT owing to the phase error

The results of IFT with the phase including random errors are shown in Fig. 5. The solid line is the result of IFT with original phases. The dash-dotted (dashed) line shows the IFT result with a random phase with a maximum error 0.4 (0.8) rad. The solid line is fitted by the two Gaussians; the standard deviation of one Gaussian is 210.1  $\mu\text{m}$  and that of the other Gaussian is 105.1  $\mu\text{m}$ . The separation of two Gaussians is 420.1  $\mu\text{m}$ . The electron beam shape with larger phase errors is distorted more than that with smaller phase errors. As expected, the asymmetric shape is reconstructed when there is no phase error. However, the shape of the electron beam is distorted when there are random phase errors. Therefore, we need to find a method to reduce the phase error in this IFT process.

### 3.3. Phase-retrieval algorithm

The algorithm of the phase-retrieval method is shown in Fig. 6. The initial starting function should be the result of the IFT shown in Fig. 5. The function obtained by the IFT in Fig. 5

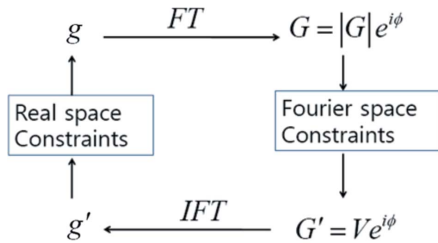


**Figure 6**  
Scheme of the phase-retrieval algorithm.

in the previous section is represented by  $g$  in Fig. 6. We first make the FT of  $g$ , and the function obtained in the Fourier space is denoted by  $G$  in Fig. 6. The amplitude of  $G$  is represented by  $|G|$ . This amplitude is replaced by the visibility  $V$  obtained in Fig. 4(a) because this visibility will be measured in the experiment. The vindication of this replacement comes from the comparison between the visibility and the amplitude of the FT, as shown in Fig. 4(a). This replacement plays the key role in this algorithm, and this process is called the Fourier space constraint.

We need one more strategy to complete the algorithm. The new function obtained after the replacement is denoted by  $G'$  in Fig. 6. By IFT we can obtain a function in real space denoted by  $g'$  in Fig. 6. This function usually has negative points. However, the electron beam distribution should not have a negative value because a negative distribution has no physical meaning. Thus, the negative points should be removed from  $g'$  changing the negative values to zero. This process is called the real space constraint.

After changing the negative values to zero, the initial function  $g$  is replaced by  $g'$ . We can iterate this process until the iteration does not show a meaningful difference from the previous step. This iteration process is called the phase-retrieval algorithm (Fienup, 1980). Note that the negative value can be replaced with an arbitrary value if there is any need to try such a strategy. In this study the simple method of changing the negative value to zero is sufficient to reconstruct the electron beam shape.

Fig. 7 shows the recovery process of the electron beam distribution according to the phase-retrieval algorithm. The dashed line represents the initial distorted function from Fig. 5 with a maximum phase error of 0.8 rad. The dash-dotted line is the recovered function after the first iteration. The solid line is the result after 2000 iterations, which is sufficient to recover the electron beam shape shown in Fig. 3. The asymmetric function is recovered with the phase-retrieval algorithm. The solid line is also fitted by two Gaussians. The standard deviation of one Gaussian is 216.3  $\mu\text{m}$  and the other Gaussian is 100.2  $\mu\text{m}$ . The separation of the two Gaussians is 426.59  $\mu\text{m}$ . Even in the case of the maximum error of 0.8 rad the recovered result is reasonably close to the electron beam shape in Fig. 3.

#### 4. Experimental study

A schematic diagram of the interferometer at the 1B1 beamline of PLS is shown in Fig. 8. The radiation generated from

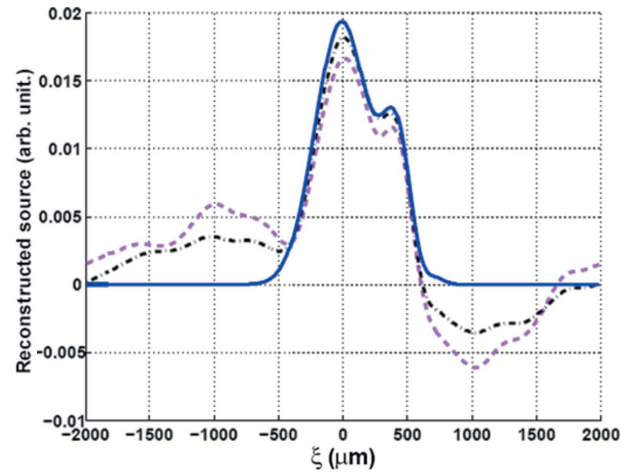


**Figure 7**  
Electron beam shape obtained by iterations. The dashed line represents the initial function with random phase errors with a maximum value of 0.8 rad, as shown in Fig. 4(b). The dash-dotted line is the reconstructed function  $g'$  after one iteration. The solid line is the result after 2000 iterations.

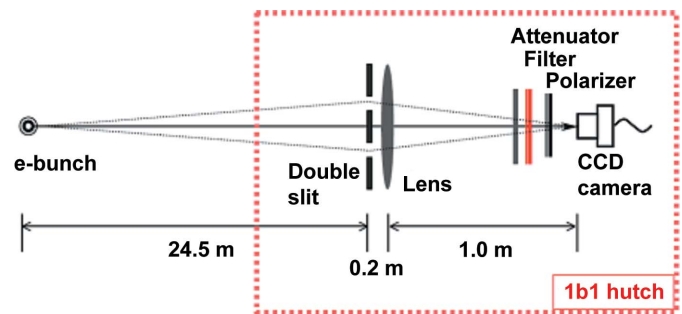


**Figure 8**  
Schematic diagram of 1B1 beamline at PLS.

the electron beam in the storage ring propagates to the end of the beamline. Three optical mirrors reflect only visible light in the transport path of the radiation to the interferometer (Huang & Ko, 1998). Note that these mirrors can be the source of phase measurement errors of the complex degree of coherency (Mitsuhashi, 1999). A commercial band-pass filter [CVI Melles Griot, 03 FIV 022 (F10-650.0-50.0M)] is used between the slit and the detector in the interferometer. The FWHM bandwidth of the optical band-pass filter is 10 nm. In the experiment, 650 nm is selected by the band-pass filter. A focusing lens is used to overlap two lights passing through each slit on the CCD plane.

#### 4.1. Measurement of visibility and phase

A measured interferogram is shown in Fig. 9 by squares. In the measurement the slit width is 500  $\mu\text{m}$ , the slit length is 6 cm and the distance  $d$  between two slits is 6 mm. The distance  $L$  between the source and the slit is 24.5 m. The fitting formula on the basis of equation (5) is given by

$$I = 2 \left[ \frac{A \sin(Bx)}{x} \right]^2 [1 + E \cos(Cx + D)], \quad (6)$$

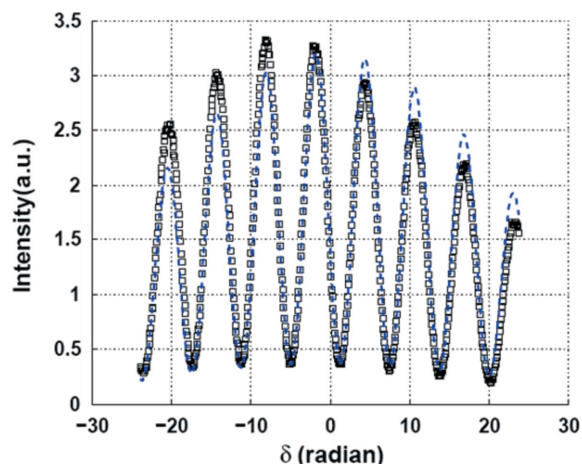


**Figure 9** Measured interferogram (squares) at PLS and the fitting result (lines) when the distance  $d$  between two slits is 6 mm. The constants for this fitting after equation (6) are obtained as  $A = 2.281$ ,  $B = 0.4145$ ,  $C = 7.995$ ,  $D = 1.817$  and  $E = 0.7943$ .

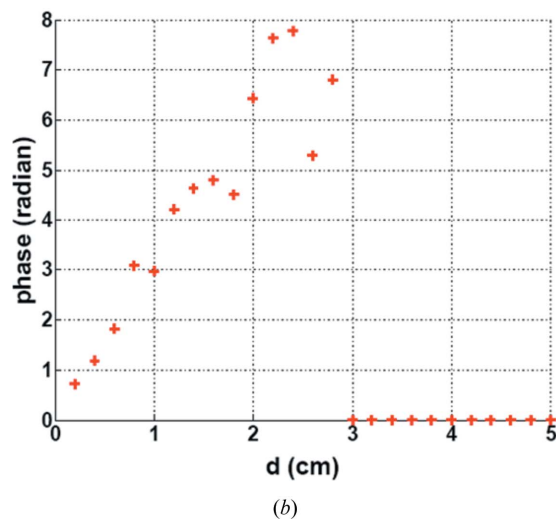
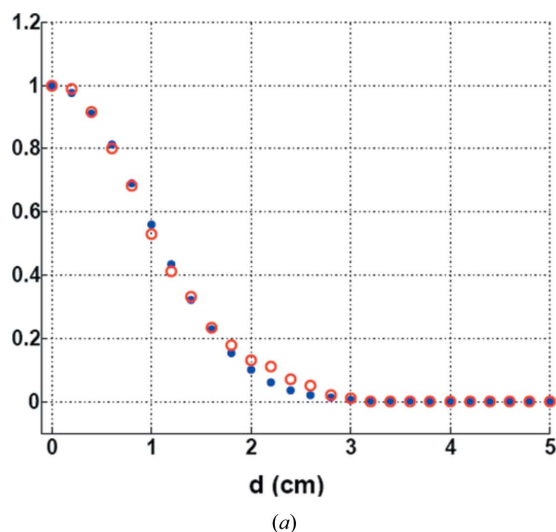


**Figure 10** (a) The circles are measured visibilities. The dots are the amplitudes of the FT of a Gaussian distribution with  $\sigma = 210 \mu\text{m}$ . (b) Measured phase.

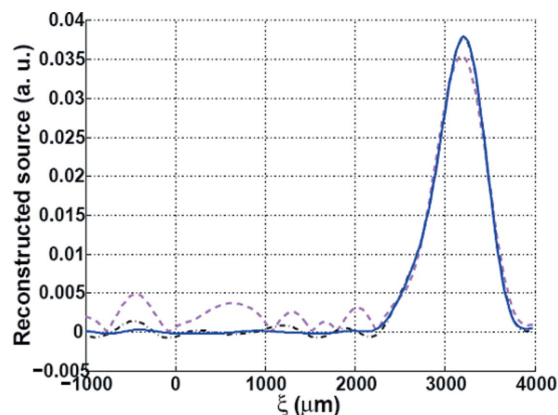


**Figure 11** Results obtained by IFT with measured visibility and phase. The dashed line represents the initial function obtained by IFT. The dash-dotted line is the reconstructed function after first iteration with the phase-retrieval algorithm. The solid line is the result after 100 iterations.

where  $x$  is the pixel position. The dotted line in Fig. 9 is the fitting line with equation (6). The constants are given for the fitting line as  $A = 2.281$ ,  $B = 0.4145$ ,  $C = 7.995$ ,  $D = 1.817$  and  $E = 0.7943$ .  $D$  is the experimental phase of the complex degree of coherency. In this fitting result  $D$ , a fitting error and measurement error exist. Our objective is to reduce this error using the phase-retrieval algorithm.

The visibilities are measured by 25 slit masks with different slit distances  $d$  and the results are represented by circles in Fig. 10(a). Note that these visibilities are not obtained from the fitting results but from the maximum and minimum values from the measured interferograms. The dots in Fig. 10(a) are the amplitudes of FT results with a single Gaussian distribution. Two results are different, which means that the electron beam distribution may be not Gaussian at PLS. The measured phase is shown by dots in Fig. 10(b).

#### 4.2. Reconstruction of electron beam shape by IFT and the phase-retrieval algorithm

The IFT result in Fig. 10 is shown by a dashed line in Fig. 11. As expected, the result is distorted (Mitsuhashi, 1999). The recovery of the electron beam is attempted by the phase-retrieval algorithm and the result is shown in Fig. 11. The dash-dotted line is the first iteration result. The result after 100 iterations is plotted with a solid line. The distribution of the electron beam at PLS is revealed as not a Gaussian distribution. This fitting result tells us that the half width at half-maximum is  $317 \mu\text{m}$ . The right-hand side of the recovered electron beam distribution in Fig. 11 can be fitted with a Gaussian function. The standard deviation of the fitted result is  $273 \mu\text{m}$ .

#### 5. Summary

A theory of interference is reviewed in order to understand the relation between the source shape and the spatial coherency of light. A random phase error is added in the phase part of the FT of the given electron distribution to simulate the

experimental situation. A distorted distribution is obtained by the IFT with a random phase error. The phase-retrieval algorithm is applied to recover the electron distribution used in the numerical study from the distorted IFT result. The phases are obtained from the fitting result of the measured interferograms. The phase errors from the fitting and experimental measure are decreased by the phase-retrieval algorithm, and the results show us that the electron distribution in PLS is not a Gaussian distribution. This technique can be applied to measure the distribution of the electron beam in fourth-generation light sources such as XFEL. This method is applicable to the reconstruction of any kinds of light sources such as stars.

This work was supported by a grant from the National Research Foundation of Korea, funded by the Korean government (Ministry of Education, Science and Technology, Korea) (grant No. 2008-0059842). This research was partly supported by the Basic Science Research Program of the National Research Foundation of Korea, funded by the Ministry of Education, Science and Technology, Korea (grant No. 2010-0008034). We would like to extend our gratitude to Dr Beom Hyun Kim (Department of Physics, Pohang

University of Science and Technology) for his assistance and discussions.

## References

- Born, M. & Wolf, E. (1999). *Principles of Optics*, 7th ed. (extended), ch. 10. New York: Cambridge University Press.
- Cittert, P. H. van (1934). *Physica*, **1**, 201.
- Fienup, J. R. (1980). *Opt. Eng.* **19**, 297–305.
- Fisher, A. S., Bong, E. L., Holtzapple, R. L. & Petree, M. (2001). *Proceedings of the 2001 Particle Accelerator Conference*, Chicago, USA, p. 547.
- Goodman, J. W. (1985). *Statistical Optics*, ch. 5. New York: John Wiley and Sons.
- Huang, J. Y. & Ko, I. S. (1998). *J. Synchrotron Rad.* **5**, 642–644.
- Masaki, M. & Takano, S. (2003). *J. Synchrotron Rad.* **10**, 295–302.
- Mitsuhashi, T. (1999). *Proceedings of the Joint US–CERN–Japan–Russia School on Particle Accelerator Beam Measurements*, pp. 399–427. Singapore: World Scientific.
- Naito, T. & Mitsuhashi, T. (2006). *Phys. Rev. ST Accel. Beams*, **9**, 122802.
- Parc, Y. W., Kim, C., Huang, J. Y. & Ko, I. S. (2009). *J. Synchrotron Rad.* **16**, 642–646.
- Sakai, I., Yamamoto, Y., Mitsuhashi, T., Amano, D. & Iwasaki, H. (2000). *Rev. Sci. Instrum.* **71**, 1264–1267.
- Zernike, F. (1938). *Physica*, **5**, 785.